Nanosecond Laser Surface Patterning of Ti6Al4V Bio-alloy for Improved Biological Performance

Sunita Kedia[1],* Shazia Shaikh[1,2], Ananda G. Majumdar[3], Mahesh Subramanian[3,4], A. K. Sahu[5], Sucharita Sinha[1,4]

[1]*Laser & Plasma Surface Processing Section, Bhabha Atomic Research Centre, Mumbai 400085, India*
[2]*University of Mumbai, Fort, Mumbai 400001, India*
[3]*Bio-Organic Division, Bhabha Atomic Research Centre, Mumbai 400085, India*
[4]*Homi Bhabha National Institute, Training School Complex, Anushaktinagar, Mumbai 400094, India*
[5]*Glass and Advanced Material Division, Bhabha Atomic Research Centre, Mumbai 400085, India*

*Corresponding authors: E-mail: skedia@barc.gov.in

Received: 02 April 2019, Revised: 11 June 2019 and Accepted: 11 June 2019

DOI: 10.5185/amlett.2019.0026
www.vbripress.com/aml

Abstract

Biological performances such as osseointegration and biocompatibility of Ti6Al4V alloy primarily depends on topological and chemical properties of the surface of the bio-material. Here, a nanosecond pulsed Nd:YAG laser has been used to generate microstructures on Ti6Al4V surface by irradiating with 6000 number of laser shots per site. Formation of ripple structure and generation of sub-oxide phases on laser treated titanium surface supported uniform and dense growth of HAP on the sample. In contrast, discrete nucleation of HAP with comparable higher precipitation of calcium occurred on untreated Ti6Al4V sample when subjected to similar in vitro tests by exposing the sample to simulated body fluid. Initial interaction and growth of U2OS cells on untreated and laser treated Ti6Al4V substrates were quantified using MTT assay. More numbers of cell were attached to laser treated sample in comparison to untreated sample as observed in confocal microscope images. Our results suggested that surface patterning of Ti6Al4V alloy using nanosecond pulsed laser promoted bio-integration without compromising its biocompatibility. Copyright © VBRI Press.

Keywords: Laser surface patterning, Ti6Al4V bio-alloy, hydroxyapatite, U2OS cell.

Introduction

Osseointegration efficiency and long-term acceptance of artificial implants within human body depend primarily on the surface properties of the implant. Lack of quality Osseo integration can lead to implant failure often requiring implant replacement. Some other factors such as, chronic inflammation at implant tissue interface, short/long term microbial infections, prolonged friction, low immune response, and mechanical stress can also lead to implant failure in human body. Roughness, wettability and chemical properties of the implant surface decide its interaction with biological fluid, thus controlling the initial attachment and proliferation of body tissues/cells on implant surface. To overcome poor performance of implants, development of different physical, chemical and biochemical techniques which can enhance surface properties of the biological implants have been in progress. Hydroxyapatite (HAP: $Ca_{10}(PO_4)_6(OH)_2$) is a body mineral which is rich in calcium and phosphorus and is known to work as an efficient bone-implant interface layer. Quality and growth of HAP layer on an implant surface decides sustainability of this foreign material i.e. implant within the human body. The very first process an implant undergoes in the body is adsorption of tissue fluid and cell binding proteins on its surface [**1**]. Nucleation and growth of HAP are regulated by quality of these proteins adsorbed onto implant surface. These early actions decide initial interactions leading to final cellular response of the implant in the body. Properties and organization of proteins on the implant depend upon roughness, wettability and chemical composition of the implant surface.

Varieties of glasses, metals, alloys, ceramics and polymers-based bio-implants have been developed and have been in use in different parts of the human body, either as a support or as a replacement [**2-4**]. Among these, titanium and its alloys are most commonly used as orthopaedic and dental implants. Titanium has high strength to weight ratio, good corrosion resistance, low density and low Young's modulus which make this metal popular as bio-implants [**5**]. However, titanium is bio-inert and it does not easily integrate with bones directly. Hence, development of HAP layer on the

titanium implant surface is a primary requirement for its acceptance inside the body. Good adhesion and complete coverage of HAP on titanium-based implants has been a main hurdle. An approach tried to overcome bio-inertness of titanium-based implants has been via surface modification of such implants. Increased micro-roughness [**6**], superior wettability [**7**] and generation of oxide phases [**8**] on titanium surface are some of the common practices which have been tried to improve performance of titanium-based implants in biological environment. Some surface treatment techniques for titanium implants include acid etching [**9**], alkaline treatment [**10**], anodization [**8**], sintering [**11**], and sandblasting [**12**]. Oh *et al.* reported significant improvement of HAP growth on anodized nano-structured titanium substrate [**8**]. Yuan *et al.* generated micro/nano hierarchical structures on titanium by etching and sand blasting techniques which resulted in improved initial stability of implants and enhanced osseointegration [**12**]. Pylypchuk *et al.* reported biomimetic approach for HAP coating on titanium [**13**]. Wang *et al.* reported enhanced osseointegration on oxidised micro-structured titanium surface [**14**]. An alternative effective method used to enhance surface properties of titanium sample involves laser induced surface modification [**7**].

Laser based micromachining has gained fast response in the field of medical devices and implants over other micro-fabrication processes due to several advantages. Laser beam has ability to precisely modify surface of the sample retaining its bulk properties. Laser surface patterning is anon-contact, single-step, controlled, fast, and reproducible technique. This provides very precise and contamination-free samples. Laser matter interactions can lead to purely physical changes resulting from thermal effects on account of absorbed laser energy by the material and associated melting and evaporation. Another effect arising from laser matter interaction involves, photon induced chemical changes occurring on the surface of the sample. Several reports have shown that presence of microstructures on the interface between the implant and body tissues improve bio-integration and protect implants from bacterial infections. Zhang *et al.* showed laser treated titanium-alloy promoted adhesion and proliferation of cultured osteoblasts [**9**]. Faria *et al.* reported superior growth of HAP on laser induced line-shaped textured titanium-alloy surface [**15**]. Mirhosseini *et al.* investigated in vitro growth of 2T3 osteoblast cell on laser treated titanium alloy surface using MTT assay [**16**].

In the study being reported, a nanosecond pulsed (ns) laser was employed for surface patterning of Grade 5 titanium-alloy (Ti6Al4V: titanium - 6 wt% Aluminium – 4 wt % Vanadium) to modify its surface properties leading to improved growth of HAP and adhesion of U2OS human osteosarcoma cells on it. Number of laser pulses irradiating the Ti6Al4V surface was optimized resulting in generation of a rough surface associated with mixed (anatase + rutile) titanium oxide phase. Investigations on topographical and physicochemical changes on Ti6Al4V alloy surface, when surface modified by irradiating an optimum of 6000 laser pulses per site were carried out in this study. Effect of surface modification on formation of HAP layer and adhesion of osteoblast human cell on laser modified Ti6Al4V surface were correlated. Formation of microstructure and generation of titanium oxide phases on laser treated sample were confirmed by Scanning Electron Microscope (SEM), X-ray Diffraction (XRD), micro-Raman analysis techniques. Laser treated Ti6Al4V and untreated Ti6Al4V samples were dipped in simulated body fluid (SBF) for 10 days to evaluate their in vitro bio-integration property. Faster and ssuperior growth of HAP in terms of thick and continuous growth with expected calcium to phosphorous ratio (Ca/P) on laser treated sample was observed. In contrast, discrete nucleation of HAP with higher precipitation of calcium was revealed on untreated sample. Initial interaction of U2OS cells with laser treated and untreated samples were examined. More number of cells attached to laser treated sample in comparison to untreated sample, as confirmed using confocal microscope images.

Experiment

Ti6Al4V samples, each of dimension of 20 mm × 20 mm × 1 mm were mechanically polished to a surface roughness of Rz = 0.2 μm followed by cleaning with acetone and de-ionized water for 5 min each in an ultrasonic bath. Laser induced surface patterning was done by employing a Q-switched Nd:YAG nanosecond pulsed laser system delivering second harmonic at wavelength 532 nm with 6 ns pulse duration and 10 Hz pulse repetition rate. Laser beam of average power ~ 40mW was focused on the sample using a 10 cm focal length lens. The focal spot diameter measured for single laser shot at sample location on a thermal paper was ~ 390 μm. This corresponds to a typical laser fluence of 0.8 J/cm^{2}incident on the sample. The number of laser pulses incident on the sample was varied to arrive at a condition where surface modification occurred with limited formation of deep craters. A surface patterning grid with circular spots 355 μm apart over a total area of 10 mm × 10 mm was obtained by translating the Ti6Al4V sample along X and Y directions using a computer controlled translational stage. Surface topography and chemical composition of laser treated sample were studied using SEM images, XRD technique and micro-Raman analysis.

The bio-active property in terms of growth of HAP on laser treated and untreated samples were evaluated by dipping the samples in simulated body fluid (SBF) for 10 days. The SBF solution was prepared by dissolving 6.547 gram per litre (gpl) NaCl, 2.268 gpl $NaHCO_3$, 0.373 gplKCl, 0.178 gpl $Na_2HPO_4.2H_2O$, 0.305 gpl $MgCl_2.6H_2O$, 0.368 gpl $CaCl_2.2H_2O$ and 0.071 gpl Na_2SO_4 in distilled water. The mixture was

buffered at pH value of 7.4 and 37 C using 6.057 gpl tris(hydroxymethyl)aminomethane and HCL. Both lasers treated and untreated Ti-alloy samples were immersed in 5 ml of SBF per day at maintained temperature of 37 C in an incubator. This was done over a period of 10 days. Replacement of SBF was done each day to provide new ions for HAP growth. After 10 days the samples were removed from SBF, washed with distilled water, dried in air and tested for SEM, Energy Dispersive X-ray spectroscopy (EDX), XRD, and micro-Raman measurements in order to characterize HAP growth.

For bio-compatibility tests of untreated and laser treated samples U2OS human osteosarcoma cells were procured from National Centre for Cell Science, Pune. Cells were maintained in Dulbecco's Modified Eagle's Medium (high glucose, Himedia Labs), supplemented with 10% fetal bovine serum. Zeiss LSM 780 microscope was used to visualize initial attachment of the cells on laser treated and untreated samples. About 10 random fields per sample were captured and quantified by the average number of nuclei per field. For light microscopy, the cells remaining in the wells after removal of the untreated and laser treated samples were fixed with 3.5% paraformaldehyde solution and stained with crystal violet, followed by qualitative examination under a light microscope. Cell viability and growth in presence of untreated and laser treated samples were measured by the MTT assay [**17**]. Quantification of cell growth in presence of laser treated and untreated samples was done from absorbance at 550 nm after MTT assay. Subsequently, the cells were stained with Phalloidin-FITC (Invitrogen) to visualize actin filaments, and Hoechst 33342 to visualize nuclei.

Results

Laser surface processing

In present work, circular patterns were generated on Ti6Al4V bio-alloy by employing a nanosecond pulsed Nd:YAG laser. The laser induced modification in surface topography and chemical composition of the sample were investigated and their effects on the biological performance of the sample were correlated.

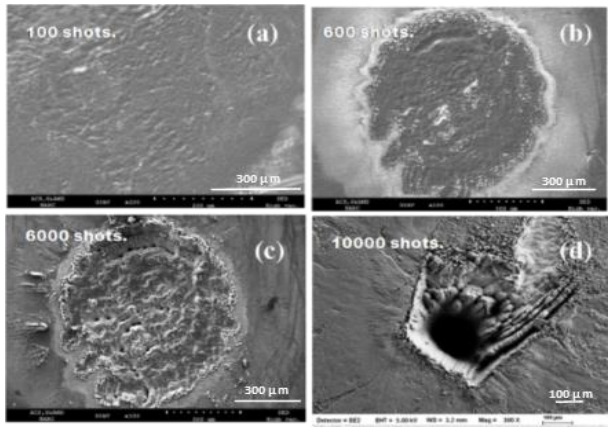

Fig. 1. SEM image Ti6Al4V sample irradiated with (a) 100, (b) 600, (c) 6000 and (d) 10000 number of laser shots.

Maintaining laser fluence of 0.8 J/cm^2, surface texturing of Ti6Al4V sample was initiated with 100 number of laser shots per site. Surface modification was not significant in this case and only the heat affected zone was observed. A visible topographical change occurred only after 600 laser shots per site which became prominent when number of laser shots was increased to 6000 pulses per site. Further increase in number of laser shots damaged the sample surface. **Figs. 1a, 1b, 1c** and **1d** show the SEM images of the sample irradiated with 100, 600, 6000 and 10000 shots per site, respectively. Hence, laser induced surface patterning obtained by irradiating 6000 laser shots per site was chosen based on our optimization runs.

Circular pattern generated using 6000 number of laser pulses was chosen to cover the full surface of the sample. **Fig 2a** shows SEM image of the sample on which circular patterns were generated in 2-dimensional grid geometry. Typical diameter of each laser induced spot was ~1000 µm and the spots were separated by ~355 µm along *x* and *y* directions. Magnified image of

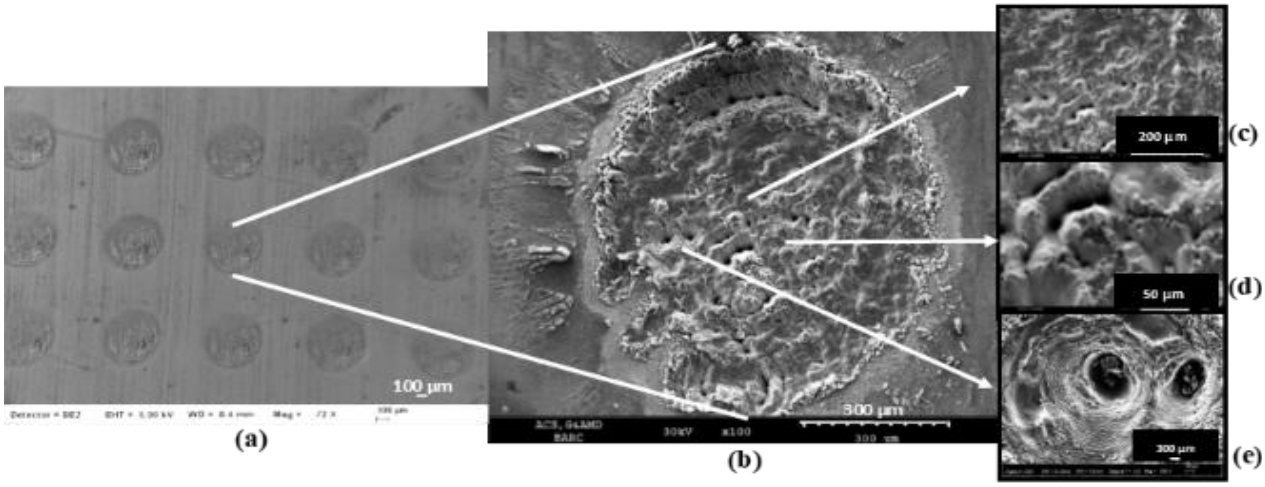

Fig. 2. SEM image of (a) laser induced circular pattern on Ti6Al4V sample generated by irradiating 6000 laser shots/site (b) magnified image of one spot (c) ripple structure, (d) conical protrusion and (e) holes due to laser spikes.

one spot in **Fig. 2b** revealed irregular rippled structures in the laser affected area. During initial stage of laser material interaction an irregular distribution of laser energy on sample surface occurred because of inbuilt roughness of Ti6Al4V surface which was measured as ~ 0.2 μm using an optical profilometer, in present case. During laser irradiation when temperature reaches melting point of titanium, melt pool was formed and molten titanium moved radially outside because of hydrodynamic motion of the liquid. This creates a spatial temperature gradient on sample surface along radial direction, as a result the liquid Ti6Al4V re-solidified because of drop in its temperature [**18**]. Thus, laser treated region has ripples with conical protrusions as shown in **Fig. 2c** and **Fig. 2d**, respectively. Elongation of these protrusions depends upon number of laser short illuminated at that location. A number of unavoidable holes were seen (**Fig. 2e**) in each circular region which occurred due to high intense spikes in incident laser beam at those locations. Surface roughness of the laser induced spots could not be measured using available optical profilometer with maximum range of 200 micron, thus indicating that the surface roughness in these regions increased beyond 200-micron post laser irradiation.

During laser irradiation, Ti6Al4V supports diffusion of oxygen through molten layer and subsequently oxidation of Ti6Al4V takes place. **Fig. 3a** is the XRD pattern of the laser treated sample. Hexagonal close packed α-phase and cubic β-phase of titanium in the sample were confirmed from JCPDS#44-1294 and JCPDS#44-1288, respectively. Additional diffraction peaks at 2θ ~ 25.3, 27.9, 41.7, 48.2, and 55.1, indicated formation of anatase (JCPDS# 84-1286) and rutile (JCPDS#88-1175) phases of titanium oxide on the sample. Diffraction peak at 43.3º corresponds to TiO phase as confirmed from JCPDS# 89-3660. Results of micro-Raman analysis shown in **Fig. 3b**, also confirmed formation of mixed anatase and rutile phases on the surface of the sample post laser treatment. Peaks at 147 cm^{-1}, 320 cm^{-1}, 398 cm^{-1}, 448 cm^{-1}, 640 cm^{-1}, and 796 cm^{-1}in **Fig. 3b**, indicated anatase phase of titanium oxide. However, peaks at 144 cm^{-1}, 235 cm^{-1}, 322 cm^{-1}, 362 cm^{-1}, 448 cm^{-1}, 612 cm^{-1}, and 827 cm^{-1} indicated rutile phase [**19**]. The fraction of anatase and rutile phases present on the laser treated sample surface was evaluated from our XRD data and a method reported by Sreekantan *et al.* [**20**]. The weight fraction of anatase to rutile phase was calculated using following formula [**20**]

$$X_A = \left(1 + 1.26\frac{I_R}{I_A}\right)^{-1} \quad (1)$$

where, X_A is the weight fraction of anatase phase, I_R and I_A are the diffraction peaks associated with the <101> plane of the anatase phase (2θ = 25.4) and <101> plane of rutile phase (2θ = 27.6) (**Fig. 3a**). Weight fraction of anatase phases in comparison to rutile phase on laser treated sample was estimated to be 42%.

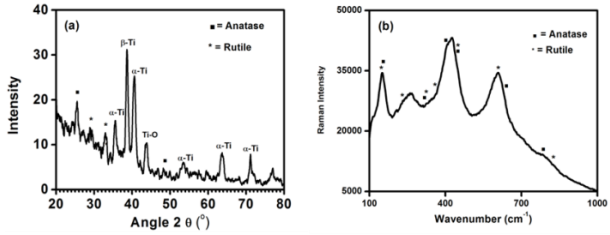

Fig. 3. (a) XRD pattern, and (b) Raman intensity of laser treated sample.

Bio-integration

For an implant, the in vitro test for formation of hydroxyapatite in simulated body fluid often works as an indicator for expected in vivo bioactivity within human body. Additional benefits of HAP coating on implant surface include faster adaptation of the implant to surrounding tissue with associated reduction in healing time, enhancement of bone formation, better implant-bone attachment, and reduction in release of toxic metallic ion [**21**].

Figs. 4a, 4b and **4c** are the SEM images of the sample laser irradiated with100 shots, 600 shots and 6000 shots, respectively and subsequently dipped in SBF just for 1 day. Discrete nucleation of HAP at different location was visible in **Fig. 4a** and **4b** as indicated with circle and ellipse, in **Figs 4a** and **4b** respectively. Relatively superior, denser and continuous growth of HAP was observed in **Fig. 4c**, as marked with squares. Our observations on better growth of HAP on sample laser treated with 6000 shots enable us to choose this condition when generating a grid pattern of several laser treated spots to cover the entire surface of the Ti6Al4V sample for our subsequent tests on bio-integration and bio-compatibility.

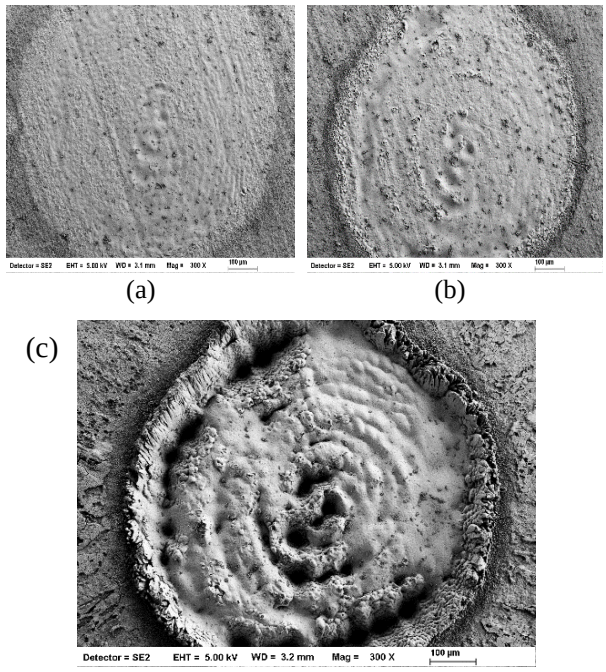

Fig. 4. SEM image of site laser irradiated with (a) 100 shots, (b) 600 shots, (c) 6000 shots and dipped in SBF for one day.

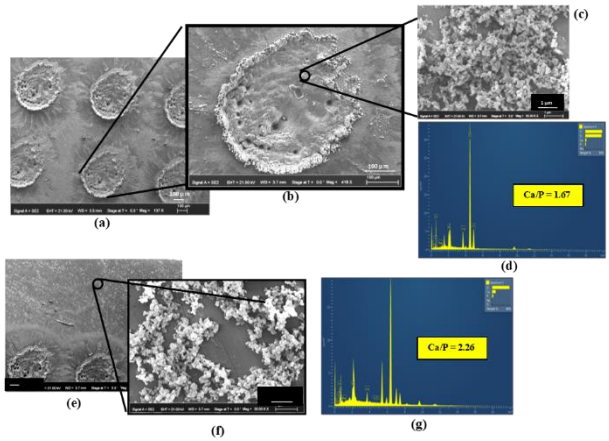

Fig. 5. SEM image of (a) laser treated sample (6000 shots/site) dipped in SBF for 10 days, (b) magnified image of one spot, (c) HAP agglomerated on laser treated region, and (d) EDX of HAP that grew on laser treated area, (e) nucleation sites of HAP on untreated sample, (f) HAP grown on untreated sample, and (g) EDX of HAP that grew on untreated sample**.**

Fig. 5a is the SEM image of laser treated sample dipped in SBF for 10 days. Uniform growth of HAP can be seen in the magnified image shown in **Fig. 5b**. Within 10 days most of the uneven region on the surface was filled with HAP and the spot looked almost smooth except the region within each of the holes. Better HAP growth can be attributed to increased surface roughness on the sample illuminated with 6000 shots per site. **Fig. 5c** shows a dense agglomeration of spherical shape HAP on laser treated sample. The calcium to phosphorus ratio (Ca/P) of HAP in this region was measured using EDX and its value was estimated to be ~1.67. The value matches with the Ca/P ratio of HAP in human body which typically lies in the range of 1.50 to 1.67 [**22**]. The rougher surface of laser treated sample provided larger surface area for interactions between Ti6Al4V and the simulated body fluid. Additionally, the micro-valley and micro-pores generated on the Ti6Al4V surface post laser treatment increased the resident time of body fluid at a particular location. Therefore, 10 days of exposure to SBF was observed to be sufficient for complete infiltration of the uneven region on the laser treated sample surface leading to formation of apatite hence, a smoother surface was observed in **Fig. 5b**. Unlike this, discrete nucleation of HAP on the untreated area of the sample was observed, as shown in **Fig. 5e**. Relatively lesser growth of HAP is seen in the magnified image, as shown in **Fig. 4f**. Ca/P ratio of HAP that grew on untreated sample was estimated to be 2.26, as shown in **Fig. 5g**. This high value Ca/P ratio was probable on account of faster precipitation of calcium on the untreated surface while ion exchange with phosphorus and formation of HAP were not efficient in this case.

Fig. 6a shows the XRD pattern of HAP that grew on laser treated sample. In XRD, the characteristic diffraction peaks representing HAP were detected at 2θ ~ 25.8°, 32.9°, 38.4°, 45.2°, 48.2°, and 51.8° (JCPDS# 09-0432). The peaks corresponding to hexagonal α-Ti, TiO phase, anatase phase), and rutile phase (JCPDS# 88-1175) of titanium dioxide were also observed in **Fig. 6a**. However, peak corresponding to cubic β-Ti was absent. Reduction of the signature peaks of titanium was because of the formation of thick HAP layer on the laser treated sample. These HAP grain sizes were typically in the range of 22-30 nm as estimated using Debye-Scherrer formula [**23**]. Complementary information was obtained from micro-Raman analysis of HAP grown on laser treated sample. **Fig. 6b** shows the Raman peak of HAP that grew on untreated and laser treated titanium sample. Raman band at 960 cm^{-1} corresponds to the symmetric stretching of P-O bonds. The vibrational band at 446 cm^{-1}, and 590 cm^{-1} are attributed to the O-P-O bending modes. Peaks at 1023 cm^{-1}, 1030 cm^{-1} and 1045 cm^{-1} corresponds to P-O asymmetric stretch and peak at 1075 cm^{-1} to theCO_3^{2-} band [**24**]. Bai *et al.* have reported better growth of HAP on surfaces containing mixed anatase and rutile phase of titanium oxide. Yang *et al.* also reported efficient growth of HAP on anatase-rutile mixed phase [**25**]. These results are in good agreement with our observations. Higher thickness, total coverage, crystallinity and fast nucleation rate of HAP layer on the laser treated surface is expected to enhance efficiency of such an implant. Both, presence of microstructures and mixed phases of titanium oxide on laser treated samples promoted faster growth of HAP in comparison to relatively smooth surface of untreated sample.

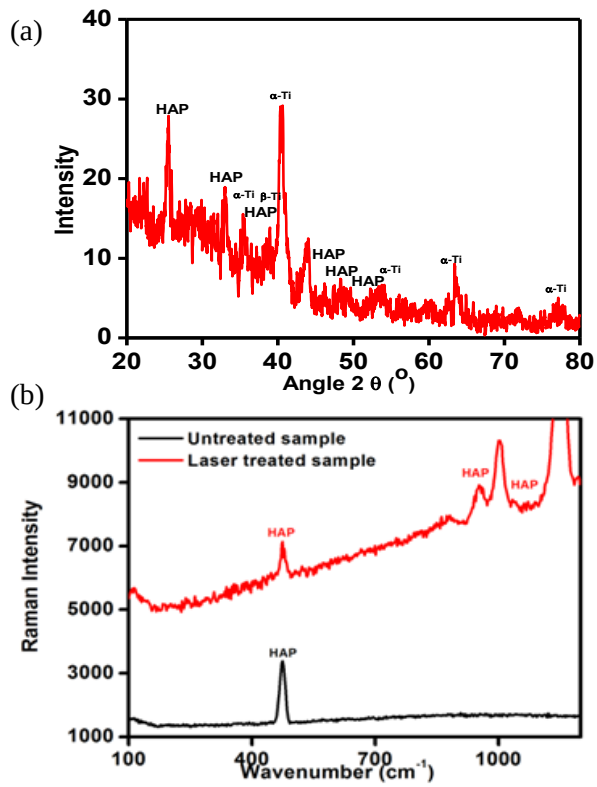

Fig. 6. (a) XRD, and (b) Raman intensity of HAP formed on untreated and laser treated sample after being dipped in SBF for 10 days.

Bio-compatibility

For our bio-compatibility tests growth and compatibility of U2OS cells on untreated and laser treated samples were compared.

Analysis of the MTT assay results demonstrated that both cell viability and growth remained unaffected in presence of either untreated or laser treated samples as shown in **Fig. 7a** and **7b**. Visualization of crystal violet stained cells under the light microscope did not yield any obvious morphological alterations either. This indicated, both untreated and laser treated samples were well accepted by U2OS human osteosarcoma cells.

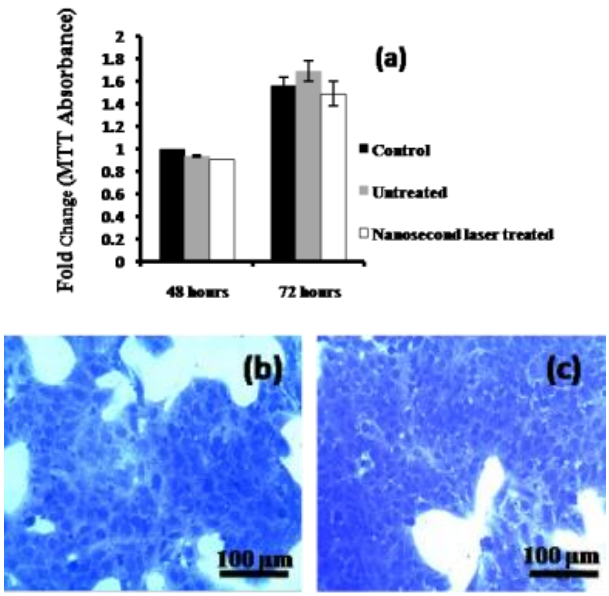

Fig. 7. (a) Absorption at 570 nm for MTT assay in presence of untreated and laser treated sample. Control data taken in absence of Ti6Al4V-alloy, Bright field microscopy of cells post exposure to (b) untreated sample and (c) laser treated sample.

Fig. 8a shows the results of growth of U2OS cells on untreated and laser treated sample surfaces estimated using confocal microscope images of cells attached to the samples. Considerable difference in attachment efficiency of U2OS cells on untreated and laser treated samples was observed. Few cells were attached to the untreated sample, while the laser treated sample showed more efficient cellular attachment on it, as shown in **Fig. 8b** and **8c**, respectively. Moreover, cell growth on the laser treated sample surface was luxurious, reaching confluence, while cells grew in isolated small patches on the untreated sample surface. This demonstrated that the laser treated sample was more conducive to the attachment and growth of osteocytes, with proliferative potential.

Phase transformation on the material surface and change in the electronic structure are responsible for the chemical properties of the surface which affects its biological behaviour [**26**]. When cells come in contact with an implant surface, the very first step that occurs is cell attachment. This is followed by cell adhesion and finally proliferation. Both cellular attachment and spreading are influenced by surface roughness and chemical compositions. Due to higher surface roughness attachment of U2OS cell on laser treated sample could have been more in comparison to untreatedsample. Brugge *et al.*, have shown poorer attachment of U2OS cells on smooth surface in comparison to rough surface [**27**]. Also, better response of MC3T3-E1 cells on rougher surface of Ti6Al4V was reported by Wu *et al.* [**28**]. Lawrence *et al.* reported enhancement in osteoblast cell proliferation on Nd:YAG laser treated Ti6Al4V alloy surface [**29**]. Aita *et al.* showed improved attachment of human mesenchymal stem cell on acid etched rough titanium surface [**30**]. Lim *et al.* have reported enhancement in cell integration on surface treated titanium alloy containing nano porous pits and thick oxide layers [**31**]. All these reports showed cells attached more readily to the rough surface in comparison to smooth surface as has also been observed in our present study.

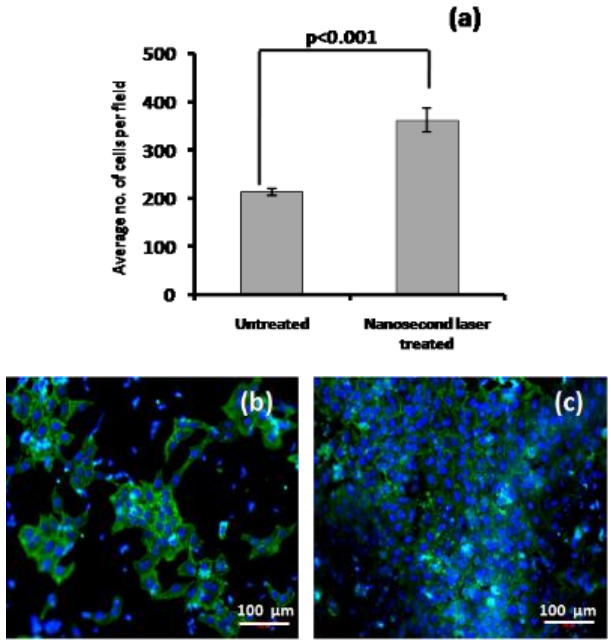

Fig. 8. (a) Quantification of growth of U2OS human osteosarcoma cells on untreated and laser treated samples, and confocal microscopy image of cells grown on (b) untreated sample and (c) laser treated sample.

Conclusion

In conclusion, laser induced circular spots in a grid pattern were generated on Ti6Al4V sample using a nanosecond Nd:YAG pulsed laser. Formation of ripple structures and formation of mixed anatase and rutile phases of titanium oxide on laser treated surface supported faster and superior osseointegration of hydroxyapatite on these lasers treated region of the sample. In addition Nd:YAG laser surface treatment also improved bio-compatibility of such sample of Ti6Al4V alloy measured in terms of higher adhesion and proliferation of U2OS osteoblast cells.

References

1. Wang, K.; Zhou, C.; Hong, Y.; Zhang, X., Interface Focus, **2012**, *2*, 259.
2. Kang, C. W.; Fang, F. Z.; *Adv. Manuf.*, **2018**, *6*, 20.
3. Saini, M.; Singh, Y.; Arora, P.; Arora, V.; Jain, K.; *World J. Clin. Cases*, **2015**, *16*, 52
4. Prakasam, M.; Locs, J.; Ancane, K. S.; Loca, D.; Largeteau, A.; Cimdina, L. B.; *J. Funct. Biomater.*, **2017**, *8*, 44.
5. Veiga, C.; Davim, J. P.; Loureiro, A. J. R.; *Rev. Adv. Mater. Sci.*, **2012**, *32*, 14.
6. Rajesh, P.; Muraledharam, C. V.; Komath, M.; Verma, H.; J. *Mater. Sci.: Mater. Med.*, **2011**, *22*, 1671.
7. Kietzig, A. M.; Hatzikiriakos, S. G.; Englezos, P.; *Langmuir*, **2009**, *25*, 4821.
8. Oh, S. H.; Finones, R. R.; Daroio, C.; Chen. L. H.; Jin, S.; *Biomaterials*, **2005**, *26*, 4938.
9. Zhang, R.; Wan, Y.; Al, X.; Wong, T.; Men, B.; *Trans. Nonferrous Met. Soc. China*, **2016**, *26*, 1019.
10. Bsat, S.; Yavari, S. A.; Munsch, M.; Valstar, E. R.; Zadpoor, A. A.; *Materials*, **2015**, *8*, 1612.
11. Brezinova, J.; Hudak, R.; Guzanova, A.; Dragonovska, D.; Izarikova, G.; Koncz. J.; *Metals*, **2016**, *6*, 171.
12. Yuan, X.; Kang, Y.; Zuo, J.; Xie, Y.; Ma, L.; Ren, X.; Bian, Z.; Wei, Q.; Zhou, K.; Wang, X.; Yu. Z.; *PLOS One*, **2018**, 1.
13. Pylypchuk, I. V.; Petranovskaya, A. L.; Gorbyk, P. P.; Korduban, A. M., Markovsky, P. E.; Ivasishin, O. M.; *Nanoscale Research Letter*, **2015**, *10*, 338.
14. Wang, G.; Li, J.; Lv, K.; Zhang, W.; Ding, X.; Yang, G.; Liu, X.; Jiang, X.; *Scientific Reports*, **2016**, *6*, 31769.
15. Faria, D.; Abreu, C. S.; Buciumeanu, M.; Dourado, N.; Carvalho, O.; Silva, F. S.; Miranda, G.; *J. Biomed Mater Res Part B*, **2018**, *106*, 1534.
16. Mirhosseini, N.; Crouse, P.L.; Schmidth, M. J. J.; Li, L.; Garrod, D.; *Appl. Surf. Sci.* **2007**, *253*, 7738.
17. Buttke, T. M.; McCubrey, J. A.; Owen, T. C.; *Journal of Immunological Methods*, **1993**, *157*, 233.
18. Sinha, S.; Singh, A. K.; *Adv. Mater. Letter*, **2013**, *4*, 492.
19. Orendorz, A.; Brodyanski, A.; Losch, J.; Bai, L. H.; Chen, Z. H.; Le, Y. K.; Ziegler, C.; Gnaser, H.; *Surface Science*, **2007**, *601*, 4390.
20. Sreekantan, S.; Hazan, R.; Lockman, Z.; *Thin Solid Film*, **2009**, *518*, 16.
21. Han, Y.; Xu, K.; *Journal of Materials Science: Materials in Medicine*, **1999,** 10, 243.
22. Kyriazis, V.; Tzaphlidou, M.; *The Scientific World Journal*, **2004**, *4*, 1027.
23. Sapra, S.; Sarma, D. D.; *Pramana J. Phys.;* **2005**, *64*, 565.
24. Ciobanu, C. S.; Massuyeau, F.; Constantin, L. V.; Predoi, D.; *Nanoscale Research Letters*, **2011**, *6*, 613.
25. Yang, B.; Uchida, M.; Kim, H. M.; Zhang, X.; Kokubo, T.; *Biomaterials*, **2004,** *25*, 1003.
26. Barthes, J.; Ciftci, S.; Ponzio, F.; Marques, H. K.; Pelyhe, L.; Gudima, A.; Kientzl, I.; Bognar, E.; Weszl, M.; Kzhyshkowska J.; Vrana, N. E., *Critical Reviews in Biotechnology*, **2018**, *38*, 423.
27. terBrugge, P. J.; Dieudonne, S.; Jansen, J. A.; *J. Biomed. Mater Res.*, **2002**, *61*, 399.
28. Wu, C.; Chen, M.; Zheng, T.; Yang, X.; *Bio-Medical Materials and Engineering*, **2015**, *26*, S155.
29. Lawrence, J.: Hao, L.; Chew, H. R.; *Surface & Coating Technology*, **2006**, *200*, 5581.
30. Aita, H.; Att, W.; Ueno, T.; Yamada, M.; Hori, N.; Iwasa, F.; Tsukimura, N.; Ogawa, T.; *Acta Biomaterialia*, **2009**, *5*, 3247.
31. Lim, Y. W.; Kwon, S. Y.; Sun, D. H.; Kim, H. E.; Kim, Y. S.; *Clin Orthop Relat Res*, **2009**, *467*, 2251.

